A direction sensitive sapphire detector for single particle detection.

O. Karacheban, M. Hempel (DESY-Zeuthen and BTU Cottbus, Germany) , K. Afanaciev (NC PHEP BSU, Minsk, Belarus), H. Henschel, W. Lange, J.L. Leonard (DESY-Zeuthen, Germany), I. Levy (Tel Aviv University, Israel), W. Lohmann (CERN, Switzerland and BTU Cottbus, Germany) and S. Schuwalow (DESY-Hamburg, Germany)

Introduction

For many applications in High Energy Physics, espetially for near-beam instrumentation, extremely radiation hard sensors are needed. Modern CVD grown diamond sensors have large variety of applications for beam diagnostics and instant luminosity measurements. Regardless of excellent radiation hardness and low noise at room temperature diamond application is limited by high cost, small size and low manufacturing rate. As an alternative we had suggested to use sapphire (aluminium oxide) detectors.

Sapphire advantages:

- industrially grown in practically unlimited amount,
- wafers have large size and low cost,
- material is radiation hardness,
- very low leakage current at room,
- signal rise time in range of few ns.

Application

Sapphire sensors have been used so far in cases where the signal is generated by simultaneous hits of many particles, i.e. in the beam halo measurement at FLASH, and are planned to be installed at FLASH II and XFEL.
Also 2 sapphire sensors were installed at CMS Beam Condition Monitor together with set of polycrystalline diamond sensors for comparison of response.

Sensors

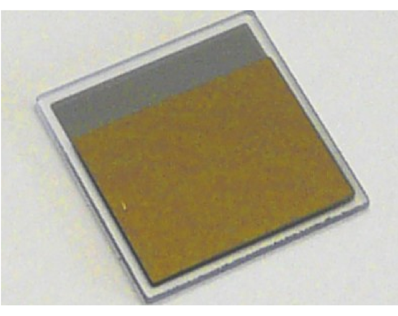

Fig.1: Metallized sapphire sensor.

An example of the metallized sapphire sensor is shown on Fig.1.
Dimensions 10 × 10 × 0.5 mm^3. Metallization from both sides with consecutive layers of Al, Pt and Au of 50 nm, 50 nm and 200 nm thickness, respectively.

Radiation hardness

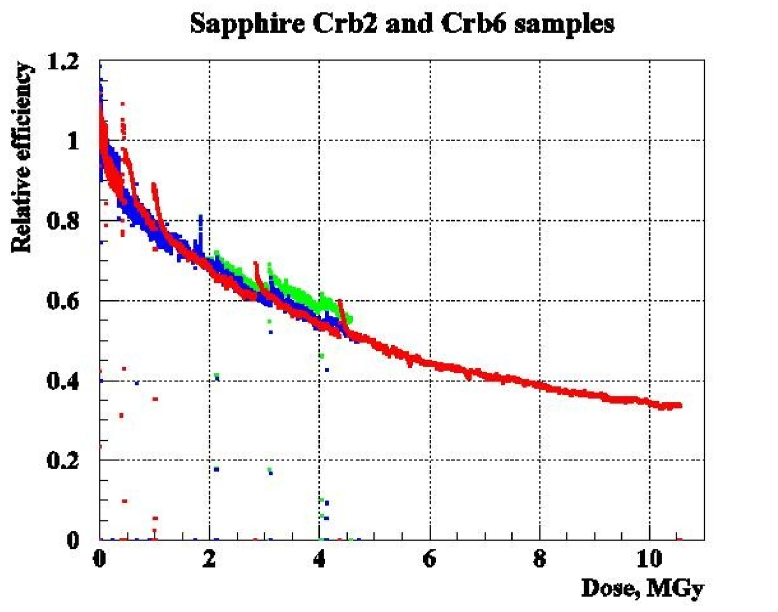

Fig.2: The relative CCE as a function of the dose in an electron beam for two sapphire samples.

Two sensors were exposed to a high-intensity electron beam at the linear accelerator DALINAC at TU Darmstadt, Germany. The beam energy was 8.5 MeV. The response of the sensors was measured as signal current. The relative drop of the signal current, interpreted as the relative drop of the Charge Collection Efficiency (CCE) is shown in Fig.2 for both sensor samples. As can be seen, the CCE degrades to about 30% of the initial CCE after a dose of 12 MGy, corresponding to more than 10 years of operation at e.g. the ILC at nominal beam parameters at 500 GeV centre-of-mass energy. The peaks on the rather smooth curves indicate an increased CCE after periods when the beam was switched off to allow other intermediate measurements or because of beam losses. When the beam was switched back on, the CCE continued to decrease. The leakage current of the sensors was measured before and after irradiation to be below 10 pA.

Sapphire detector stack design

Industrially produced sapphire has standard wafer quality, no special treatment. Therefore some impurities are always present, which leads to a decrease in the CCE.

For a CCE of about 10% of industrially produced sapphire, the signal expected for particles crossing a plate of 500 µm thickness perpendicular to its surface is only about 1100 e. This signal size is on the level of noise and can not be detected. However, if the particle crosses the sapphire sensor parallel to the 10 × 10 mm^2 metallized surface, as shown in Fig.3, the signal is enhanced by a factor 20, amounting to about 22000 e, comparable to the one in currently used solid state detectors. Therefore the orientation of the sapphire plates in the test beam was chosen to be parallel to the beam direction.
In addition, chosen orientation leads to a **direction sensitivity**. Only particles crossing the sensor parallel to the surface create the maximum signal. To increase the effective area of the detector, eight plates were assembled together. To allow wire bonding connections to the high voltage and to the readout electronics, the plates were alternatively shifted to both sides, as can be seen in Fig.4.

Readout

Each readout channel served two plates. All sensers are metallized on one side the metallization has a square shape of 9 × 9 mm^2 area, on the opposite side the metallization area is 9 × 7 mm^2 with 9 mm parallel to the beam direction, as shown in Fig.4. This way an accidental contact of high voltage wire bonds with the readout pad on the adjacent sensor is excluded. The total height of the stack was 4.2 mm with 7 mm overlap of the metal pads, leading to a sensitive area of 29.4 mm^2. The sensors were mounted inside a plastic frame as shown in Fig.5. The wire bonds for high voltage and readout connections are seen at the left and right side, respectively, in Fig.4 and Fig.5.

The leakage current of each pair of sensors was measured in laboratory to be below 10 pA at 1000 V.

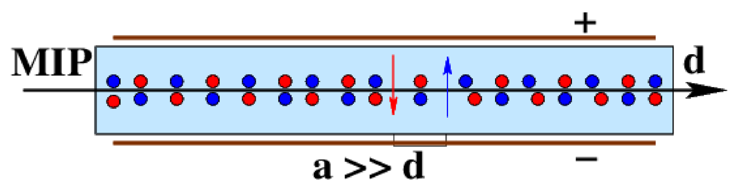

Fig.3: Orientation of single sapphire sensor with respect to the beam.

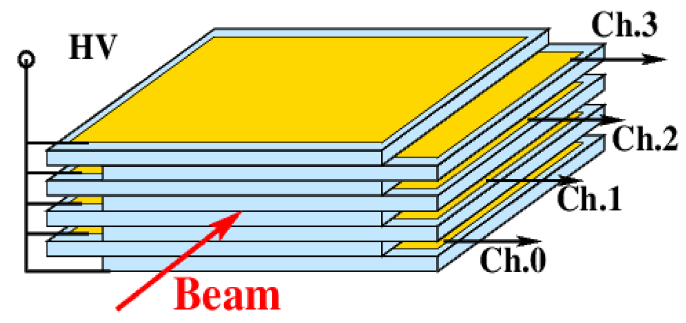

Fig.4: Schematic view of detector stack consisting of eight metallized sapphire sensors.

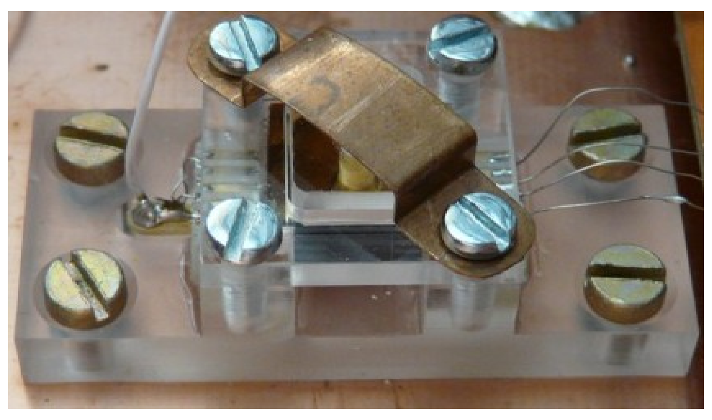

Fig.5: Assembled detector stack as used in the test beam at DESY-II.

Test beam setup, DESY-II

The stack was mounted in the middle of six planes of the EUDET pixel telescope in the 5 GeV electron beam of the DESY-II accelerator. Signals from sensors were amplified and shaped by charge sensitive preamplifiers A250 and standard RC-CR shapers with a peaking time of 100 ns and digitised by a 500 MS/s flash ADC v1721.
Two pairs of scintillators, shown as light blue planes in Fig.6 upstream and downstream of the telescope, were used as trigger to readout the telescope and the sensors. The EUDET telescope is instrumented with Mimosa 26 sensors, comprising 576 × 1152 pixels each, with a pixel size of 18.4 × 18.4 µm. The telescope planes were grouped. Planes 1−3 form the first arm, and planes 4−6 the second arm. Tracks of beam electrons were reconstructed for each group separately. From special alignment runs the width of residual distributions was measured to be below 4 µm. From a Monte Carlo study the maximum displacement of the trajectory of a 5 GeV electron due to multiple scattering in the stack was estimated to be 10 µm.

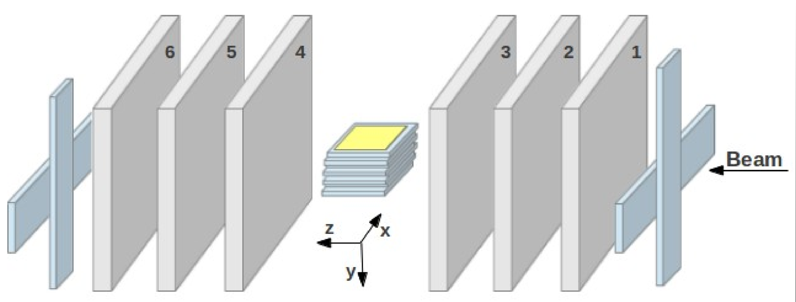

Fig.6: Sketch of the test beam setup. The sapphire stack was mounted in the middle of the 6 planes of the EUDET telescope. Crosses of two scintillators upstream and downstream of the telescope were used as the trigger for the DAQ.

Data synchronization and analysis

Stack and telescope data synchronization

For the synchronization of the EUDET telescope and the stack readout a dedicated trigger logic unit, TLU, was used. For each trigger the TLU distributed a trigger sequence to the EUDET telescope and the stack data acquisitions, such that a unique correspondence between records from both readouts was ensured.

Telescope data analysis

The standard telescope analysis software was used to convert hits in the EUDET telescope into space-points in the user geometry with the origin of the coordinate system as shown in Fig.6. Events with more than one track candidate in the telescope, amounting to about 30%, were rejected. For the remaining events the track fit was done separately for the first and second arm of the telescope. The two reconstructed tracks are considered to originate from the same beam electron if their distance in the z = 0 plane was less than a predefined cut.

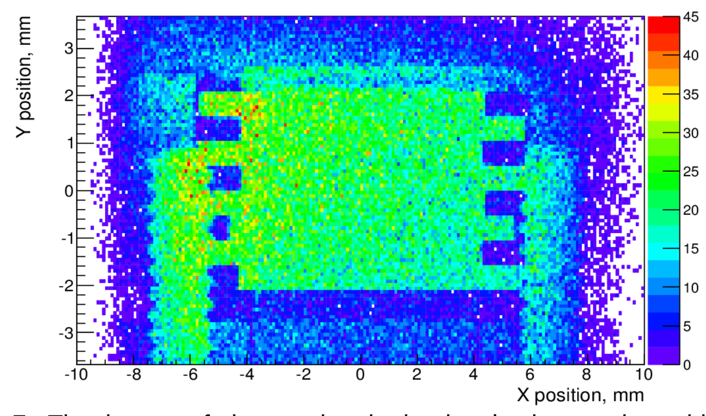

Fig.7: The image of the stack, obtained selecting tracks, which correspond to particles with big scattering angle

To determine the precise position of the stack in the beam, events with a large angle between the tracks of the first and second telescope arm were used. Requiring this angle to be larger than 0.5 mrad, an image of the stack in the xy plane at z = 0 is obtained, as shown in Fig.7. From the precise position of each plate geometrical cuts were applied to select hits in each readout channel separately. Counting plates in Fig.7 from top to bottom, the top two plates correspond to readout channel 0.

ADC data analysis

For tracks, pointing into the detector active area, signals from the ADC were averaged over a large number of triggers. Events with tracks not pointing into detector were used to study common mode noise.
Correlation between baseline values were investigated for all combinations of channels using the baseline values calculated in a predefined time window. These correlations were used in the further analysis for common mode noise subtraction. The averaged ADC output assigned to tracks not pointing into the detector was used to subtract the baseline from the averaged signal. As an example, the results for bias voltages of 550 V and 950 V are shown in Fig.8.

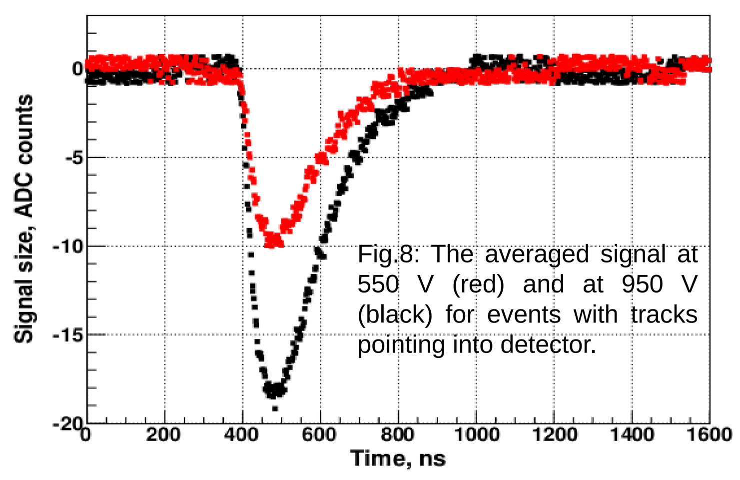

Fig.8: The averaged signal at 550 V (red) and at 950 V (black) for events with tracks pointing into detector.

Charge collection efficiency

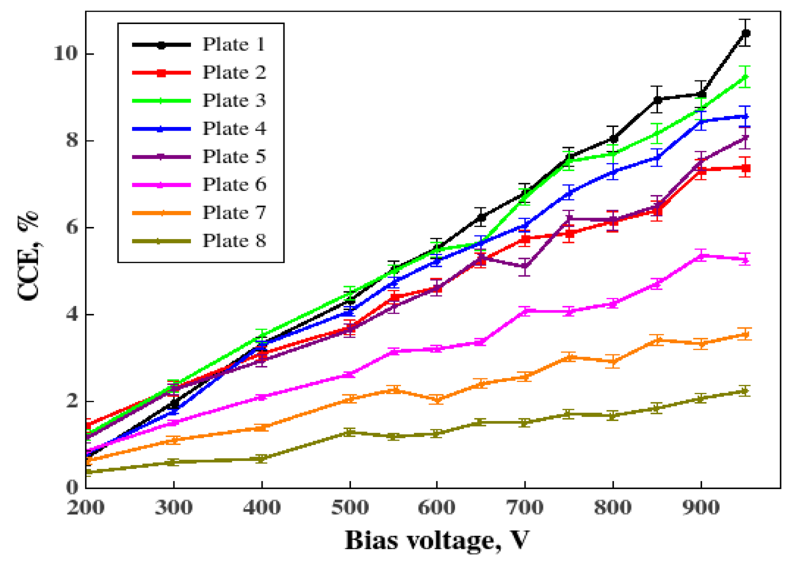

Fig.9: Measurement of the mean charge collection efficiency for eight sapphire plates as a function of the bias voltage.

The CCE is defined as ratio of the measured to the expected signal charge. The signal charge is obtained by the integration of the ADC output over a 50 ns time interval in the range [420; 470] ns. This time interval is less than the signal length as shown in Fig.8, but the RMS of the common mode noise in this range is low in comparison to the one in the tail of the signal. The mean value of the distribution of the signal charge was used for the CCE calculation at each bias voltage value.

Calibration

In order to convert the mean value into a charge each channel was calibrated by injecting a known charge into the preamplifier input. The expected amount of generated electron-hole pairs is estimated from the mean value of the ionisation energy loss inside the sensor, obtained from a GEANT simulation, and taking 27 eV as the energy needed to create an electron-hole pair.

Measurement results

The measured CCE is shown in Fig.9 as a function of the bias voltage for all plates of the stack. For each voltage value a statistics of 100000 triggers was used. To avoid an influence of metallization edges only the central part of stack was used for CCE calculation, −3 mm < x < 3 mm. An almost linear rise of the CCE is observed, reaching at 950 V e.g. for plane 1 a value of 10.5%. As can be seen, 5 out of the 8 sensor plates have a relatively high and similar CCE of about 7 − 10%, while three other plates have lower and different CCE values. As sensors did not pass any quality preselection, it can explain difference in CCE.

Theoretical model for the charge collection efficiency of sapphire sensors

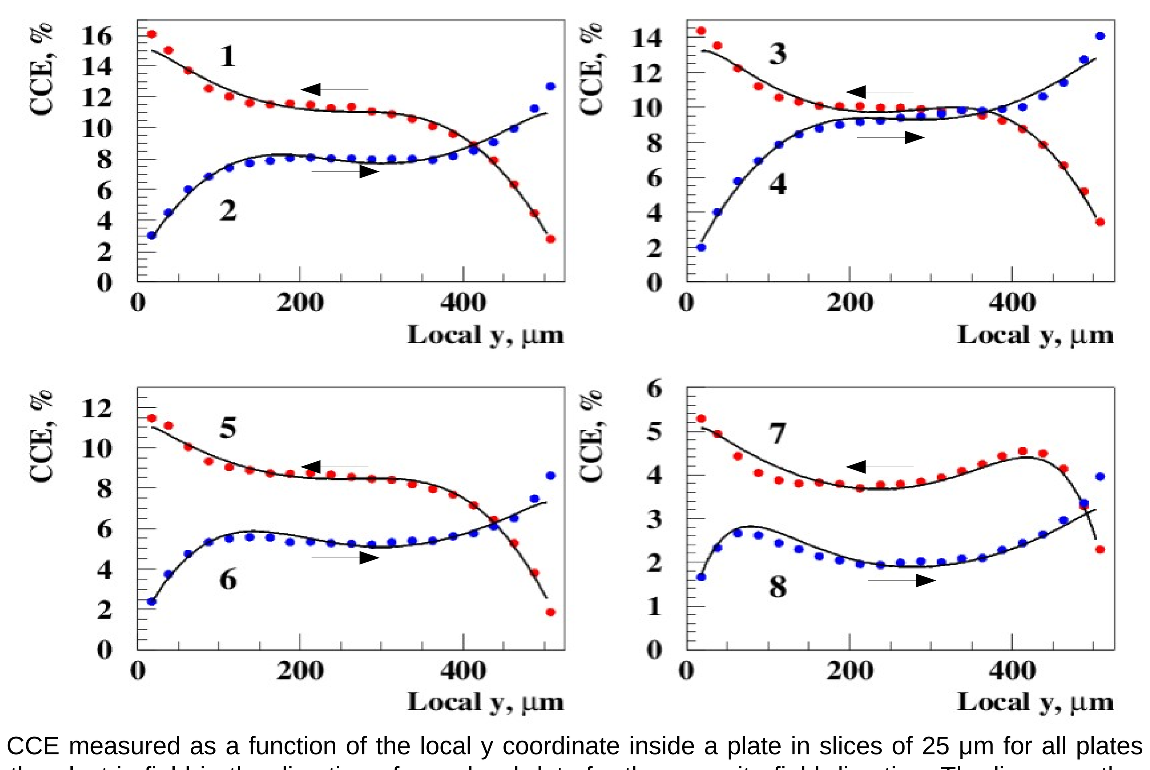

Fig.10: The CCE measured as a function of the local y coordinate inside a plate in slices of 25 µm for all plates of the sapphire stack. Blue dots are for the electric field in the direction of y and red dots for the opposite field direction. The lines are the result of a fit including both electron and hole drift. The fit parameters are given in Table 1.

Plate number	B, V /µm	f_d , %	µτ (e), $µm^2$ /V	µτ (e), $µm^2$ /V	$χ^2$
1.327 ± 0.012	52.9 ± 0.5	79.1 ± 1.1	79.1 ± 1.1	4.2 ± 0.3	19
1.255 ± 0.011	47.1 ± 0.5	59.5 ± 0.9	59.5 ± 0.9	6.2 ± 0.3	41
1.307 ± 0.010	53.3 ± 0.5	64.9 ± 0.9	64.9 ± 0.9	6.4 ± 0.2	27
1.287 ± 0.011	48.1 ± 0.5	74.6 ± 1.0	74.6 ± 1.0	3.3 ± 0.3	27
1.421 ± 0.010	47.1 ± 0.7	62.9 ± 1.0	62.9 ± 1.0	3.2 ± 0.4	16
1.342 ± 0.013	43.5 ± 1.3	39.4 ± 1.2	39.4 ± 1.2	5.1 ± 0.4	42
1.484 ± 0.010	50.1 ± 1.2	22.0 ± 0.8	22.0 ± 0.8	3.7 ± 0.4	19
1.330 ± 0.010	40.7 ± 1.7	15.1 ± 0.5	15.1 ± 0.5	3.2 ± 0.4	33

Table 1: Fit parameters for the case of electrons and holes contribution.

A linear model was developed to describe the CCE as a function of the local y coordinate inside a plate. Charged particles cross the sensor and ionize the atoms along their path through the sensor of thickness *d*. N_0 electron-hole pairs are produced. Some charge carriers will recombine immediately. A fraction of both types of charge carriers, called f_d , start to drift to the corresponding electrodes when an external electric field is applied. During the drift charge carriers may be trapped and released only after some time. The space charge due to trapped charges generates an internal electric field, called polarization field. Assuming that the space charge density will be a linear function of the local y, the resulting electric field has a parabolic shape. To estimate the signal size electrons and holes will be considered separately, as they may contribute to the resulting signal differently. Lifetime of both charge carrier is assumed to be constant. According to Ramo's theorem the signal charge *Q* is parametrised as integral from the carrier generation point y_0 to the detector edge of the differential contribution to the observed signal:

$$Q(y_0)=\frac{e\cdot f_d\cdot N_0}{d}e^{\frac{\arctan\left(\left(y_0-\frac{d}{2}\right)\sqrt{\frac{A}{B}}\right)}{\mu\tau\sqrt{AB}}}\int_{y_0}^{d}-e^{\frac{\arctan\left(\left(y-\frac{d}{2}\right)\sqrt{\frac{A}{B}}\right)}{\mu\tau\sqrt{AB}}}dy.$$

A and *B* are parameters the electric field, the quantity *B* is the electric field strength at the plane in the middle of the plate, *y = d/2*, and *µτ* is the drift path length of the electrons or holes in the electric field of unit strength. The ratio Q/N_0 is then the fraction of the charge carriers contribution to the observed CCE.
Fig.10 shows the CCE as a function of the local y coordinate, measured in 25 µm slices, together with a fit using described parametrisation. The electric field has opposite direction for adjacent plates. For example, y = 0 µm of plate 1 and y = 525 µm of plate 2 correspond to the same readout electrode.
In plates 1, 3, 5 and 7 the electric field is directed from y = 525 µm to y = 0 µm and the CCE is shown in red dots. In plates 2, 4, 6 and 8 the field direction is opposite, and the CCE is shown in blue dots. The parameters of the fit are listed in the Table 1. As can be seen, the drift length of electrons is in most of the cases more than 10 times larger than the drift length of the holes at roughly the same field strength. This result is consistent with low hole mobility and confirms the dominant contribution of electrons for the charge transport in sapphire.

Conclusions and outlook

Results of the performance of a multi channel sapphire stack in a 5 GeV electron beam are presented. It is fisrt sapphire detector, designed for single particle detection.

The CCE shows a linear dependence on the bias voltage reaching up to 10% at 950 V. A measurement of the CCE as a function of the local y coordinate through the thickness of the plates shows a pronounced dependence on y. The measurement can be explained by a linear model pointing to a dominant contribution of electron drift to the signal charge and polarisation inside the bulk of the sensor. In addition, a fraction of charge carriers of about 50% recombines immediately after creation.

These results will be used for the design of next generation sapphire detector with non-uniformity compensation.

Brandenburgische Technische Universität Cottbus - Senftenberg
EUTelescope
EUDET
AIDA
HELMHOLTZ ASSOCIATION